

Spatiotemporal control of entangling gates on atomic N -qubit systems

Ignacio R. Sola*

Departamento de Química Física, Universidad Complutense, 28040 Madrid, Spain

Seokmin Shin

School of Chemistry, Seoul National University, 08826 Seoul, Republic of Korea

Bo Y. Chang[†]

*School of Chemistry, Seoul National University, 08826 Seoul, Republic of Korea and
Research Institute of Basic Sciences, Seoul National University, 08826 Seoul, Republic of Korea*

We use a novel optimization procedure that includes the temporal and spatial parameters of the pulses acting on arrays of trapped neutral atoms, to prepare entangling gates in N -qubits systems. The spatio-temporal control allows treating a denser array of atoms, where each pulse acts on a subset of the qubits, potentially allowing to speed the gate operation by two orders of magnitude by boosting the dipole-blockade between the Rydberg states. Studying the rate of success of the algorithm under different constraints, we evaluate the impact of the proximity of the atoms and, indirectly, the role of the geometry of the arrays in 3 and 4-qubit systems, as well as the minimal energy requirements and how this energy is used among the different qubits. Finally, we characterize and classify all optimal protocols according to the mechanism of the gate, using a quantum pathways analysis.

I. INTRODUCTION

Atoms trapped by optical tweezers [1–5], interacting through Rydberg blockade [6–10], can be used to generate few multi-particle entanglement [11–21] and simple quantum circuits [16, 22–35]. However, to go further in the quest of the quantum computer [36, 37], one needs to improve the system addressability and controllability [38].

While technology has evolved to control the position of the atoms in optical traps with great precision in arrays of any dimension, current setups typically use ordered arrays of largely separated atoms, which form independent qubits. Entangling gates, based on the dipole-blockade mechanism, with energy d_B , require time durations larger than $\hbar d_B^{-1}$, and hence operate in time-scales near the microsecond regime for atoms separated over $\gtrsim 5\mu\text{m}$. Optimal control theory can be used to find efficient and robust pulse sequences [39–42], but in spite of increasing the complexity of the pulse features in the time domain, it remains very challenging to accelerate the gates without changing the setup [43, 44]. We have recently proposed a different approach to deal with this problem by controlling not only the time-domain features of the pulses but also the spatial profiles of the laser beams or the position of the atoms with respect to the fields, acting over relatively close, but no longer independent, qubits.

In the first application of the spatio-temporal control of the qubits, we proposed the symmetric orthogonal protocol (SOP), where all the *odd*-numbered pulses as well as all the *even*-numbered pulses in the sequence, are time-

delayed replicas [45]. The gate mechanism relied on the presence of a dark state in the Hamiltonian, for which even and odd pulses had to be, in a certain sense, orthogonal to each other. Then we developed a general mechanism analysis of the gates in terms of quantum pathways and we showed that by optimizing the fields with fewer constraints, a plethora of different optimal protocols with very high fidelities could be obtained, classified, and ranked, according to their dynamics [46].

In this work, we generalize our approach to treat different 2-qubit and 3-qubit entangling gates in N -qubit systems. Instead of searching and studying a single realization of the gate, *e.g.* the highest-fidelity protocol, we use quantum optimal control techniques to scan and characterize the full space of optimal solutions [32, 47–49]. The rate of success of the algorithm over a very broad sample of initial conditions is analyzed as a simple measure of the density (and quality) of solutions for different constraints in the space of parameters. We further study the mechanisms under which every optimal protocol over a broad family of pulse sequences operates using quantum pathways, and rank the protocols following the procedure recently proposed in [46].

Analyzing the overall patterns of the optimal protocols, we seek to answer questions like: What is the minimal energy introduced through external fields necessary for the gates to operate? And how much per qubit? Are all qubits used equally during the gate dynamics? How much does it depend on the type of gate or on the number of qubits in the system? And finally, can we infer which qubit arrangements or geometries are more promising for high fidelity gates?

* corresponding author: isolarei@ucm.es

[†] corresponding author: boyoung@snu.ac.kr

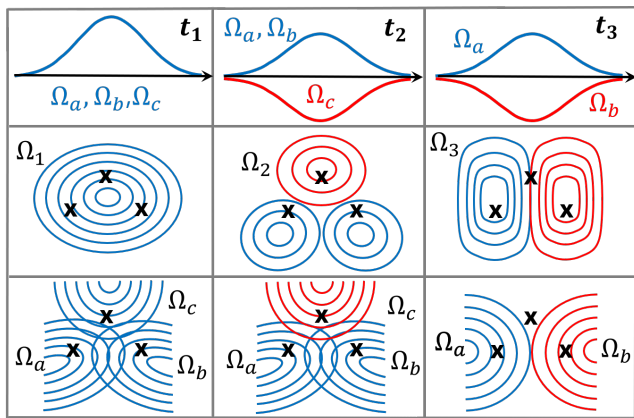


FIG. 1. Scheme showing two possible implementations of the spatio-temporal control of trapped qubits, located at the \times positions, using phase-locked Gaussian beams TEM_{00} centered at each qubit, $\Omega_a, \Omega_b, \Omega_c$ (second row) or structured pulses Ω_k whose spatial profile at the qubits coincides with the linear combination of TEM_{00} (third row). The sequence of operations that governs the temporal evolution of the state depends on the pulse sequence, shown in the first row.

II. PLATFORM SETUP AND ANALYTICAL MODEL

As a quantum platform for information processing, we consider a set of closely separated atoms trapped by optical tweezers, where the computational states are encoded in low-energy hyper-fined states, while the entangling gates (CZ or similar), which imply population return with a sign flip conditional on the state of the control qubit, use the dipole-blockade mechanism to gain a phase accumulation during the dynamics through a Rydberg state of the atom. With strong magnetic fields, the energy splitting between the qubit states can reach almost $\Delta \sim 10$ GHz [14, 50], while the energy difference between adjacent Rydberg states when the principal quantum number is around $n \sim 70$, is typically larger[51]. Therefore, in setups where the atoms are close enough that the dipole-dipole interaction is on the order of the energy splitting, $d_B \sim \Delta$, the gates can operate in the nanosecond time-scale. The price to pay is the need to find protocols that are robust under the parallel excitation of several qubits. In this work, we use the spatio-temporal control procedure to achieve precisely this goal. While the number of atoms in typical traps can easily reach the hundreds, only a small subset can be excited by the same laser pulses at the same time. They represent the minimal unit that must be controlled to engineer the gate. Here we consider subsets of 2 to 4 qubits.

In this work, we generalize the Hamiltonian and time-evolution operators to treat different entangling gates in N -qubit systems, under the same approximations used in [45] and [46]. We model the effect of the field overlapping several qubits by defining Rabi frequencies $\tilde{\Omega}_{jk}(\vec{r}_j, t) = c_{jk}\mu_{0r}E_k(t)/\hbar = c_{jk}\Omega_k(t)$, that depend on

geometrical factors $c_{j,k}$, which give the local effect of the field $\Omega_k(t)$ on the qubit j . The geometrical factors can be partially incorporated into the Franck-Condon factor μ_{0r} so we can assume, without loss of generality, that c_{jk} are normalized to one for each pulse, ($\sqrt{\sum_j c_{j,k}^2} = 1$ for all k). It is convenient to define the row vector $\mathbf{e}_k^T \equiv \langle \mathbf{e}_k | = (e_{1k}, e_{2k}, \dots, e_{nk})$ ($\mathbf{e}_k \equiv |\mathbf{e}_k\rangle$) is the column vector in bracket notation) formed by all the $e_{i,k}$ geometrical factors of a given pulse. We will call \mathbf{e}_k the *structural vectors*. From the temporal point of view, we control $\Omega_k(t)$. In this work only the pulse areas and the length of the sequence of non-overlapping pulses will be important [19–21, 52–54]. Control may be extended to other variables, including the time-delays and the relative phases between the pulses [47–49, 55–61].

The spatial control is encoded in \mathbf{e}_k and can be achieved by different means. In [45] we proposed the use of hybrid modes of light to allow a wide range of possible values for \mathbf{e}_k , including negative amplitudes. A possible generalization for spatially non-orthogonal pulses may require more complex structured light[62], such as those sketched in Fig.1 (second row). A simpler laboratory implementation, shown in the third row, can be achieved using a superposition of overlapping phase-locked Gaussian modes centered at different qubits, instead of a single field, for each pulse in the sequence. In any case, it is necessary to dispose of sufficiently complex light structures to extend the control to the spatial domain [63, 64]. A different alternative could be achieved by moving the atoms to different positions, but this would slow down significantly the gate duration.

For each qubit, there are 2 states that form the computational basis, which are the states that can be initially populated, and an additional Rydberg state, so the full Hilbert space can be spanned by 3^N states.[36] In the strong dipole-blockade regime, where only a single qubit can be excited to a Rydberg state, the number of states that can be populated during the dynamics is $2^N + N 2^{N-1}$, forming 2^N disconnected systems (the Hamiltonian is a block matrix under the approximations considered in the model), that can be classified as:

- A $V^{(N,1)}$ subsystem formed by the ground state $|0 \dots 0\rangle$ coupled to the N Rydberg excitations $|0 \dots r_e \dots 0\rangle$ by $c_{e,k}\Omega_k$, where e can occupy the positions 1 to N ($1 \leq e \leq N$).
- N $V^{(N-1,m)}$ subsystems formed by the single-excited qubit states $|0 \dots 1_h \dots 0\rangle$ ($1 \leq h \leq N$), each coupled to the $N - 1$ Rydberg excited states $|0 \dots r_e \dots 1_h \dots 0\rangle$ ($e \neq h$) by $c_{e,k}\Omega_k$. The second index m distinguishes the N different $V^{(N-1,m)}$ structures which differ by the states that are participating. We order them choosing the index m as the excited qubit h , so that for $m = 1$ the “ground” state is $|10 \dots 0\rangle$ and the remaining $N - 1$ states are $|1r \dots 0\rangle, \dots |10 \dots r\rangle$.
- $N!/(N_e!(N - N_e)!) V^{(N-N_e,m)}$ subsystems formed

by the N_e -excited qubit states coupled to their possible Rydberg excitations.

- \vdots
- N two-level systems ($V^{(1,m)}, m \in [1, N]$) with $|1 \cdots 0_e \cdots 1\rangle$ and $|1 \cdots r_e \cdots 1\rangle$
- The uncoupled N -excited qubit state $|1 \cdots 1\rangle$ ($V^{(0,1)}$ system).

We can treat the dynamics of each subsystem independently, but the outcome must be conditioned to the logic of the entangling 2 (or 3) qubit gate. We consider the following version of the CZ gate, \mathcal{P}_{ab} , acting on qubits a and b (a is by definition the first qubit, b the second) with logic tableaux $|00 \cdots\rangle \rightarrow -|00 \cdots\rangle$, $|01 \cdots\rangle \rightarrow -|01 \cdots\rangle$, $|10 \cdots\rangle \rightarrow -|10 \cdots\rangle$, $|11 \cdots\rangle \rightarrow |11 \cdots\rangle$, regardless of the values of any additional qubits c, d , etc. The set of conditions can be summarized in the diagonal elements of the matrix \mathbf{P}_{ab} . For instance, in a 3-qubit system, the \mathcal{P}_{ab} has the signature $\text{diag}\{-1, -1, -1, -1, -1, -1, 1, 1\}$ for a basis ordered as $|000\rangle, |001\rangle, |010\rangle, |100\rangle, |011\rangle, |101\rangle, |110\rangle, |111\rangle$.

In addition to studying the optimization of the \mathcal{P}_{ab} gate, we also consider 3-qubit entangling gates as \mathcal{P}_{abc} , where the matrix \mathbf{P}_{abc} is diagonal with signature $\text{diag}\{-1, -1, -1, -1, -1, -1, -1, 1\}$.

For non-overlapping pulses with single-photon Rabi frequency $\Omega_k(t)$, in the rotating-wave approximation and in the interaction picture, the Hamiltonian is a direct sum of subsystem $V^{(n,m)}$ Hamiltonians, $\mathbf{H}_k^{(n,m)}(t)$, which are everywhere zero except for the first row/column, with matrix elements $H_{k,11}^{(n,m)} = 0$ and $H_{k,1j}^{(n,m)}(t) = -c_{j-1,k}\Omega_k(t)/2$ ($j = 2, N$), where t is defined within the domain of the pulse k .

For each $V^{(n,m)}$, the time-evolution operator is a $(n+1) \times (n+1)$ matrix that can be written as a time-ordered product of the time-evolution operators for each pulse in the sequence,

$$\mathbf{U}_T^{(n,m)} = \prod_{k=0}^{N_p-1} \mathbf{U}_{N_p-k}^{(n,m)}$$

where

$$\mathbf{U}_k^{(n,m)} = \begin{pmatrix} \cos S_k^{(n,m)} & ie_{1,k} \sin S_k^{(n,m)} & ie_{2,k} \sin S_k^{(n,m)} & \cdots & ie_{n,k} \sin S_k^{(n,m)} \\ ie_{1,k} \sin S_k^{(n,m)} & 1 + e_{1,k}^2 [\cos S_k^{(n,m)} - 1] & e_{1,k}e_{2,k} [\cos S_k^{(n,m)} - 1] & \cdots & e_{1,k}e_{n,k} [\cos S_k^{(n,m)} - 1] \\ \vdots & \vdots & \vdots & \ddots & \vdots \\ ie_{n,k} \sin S_k^{(n,m)} & e_{n,k}e_{1,k} [\cos S_k^{(n,m)} - 1] & e_{n,k}e_{2,k} [\cos S_k^{(n,m)} - 1] & \cdots & 1 + e_{n,k}^2 [\cos S_k^{(n,m)} - 1] \end{pmatrix} \quad (1)$$

where the geometrical factors, $e_{j,k} = c_{j,k}/f_k^{(n,m)}$, are normalized with

$$f_k^{(n,m)} = \sqrt{\sum_{i \in m} c_{i,k}^2}, \quad (2)$$

that depend on the subsystem through the coefficients that enter in $f_k^{(n,m)}$. The general form of the propagator is, however, independent of the m index. If $n = 1$, $c_{1,k}$ can only be ± 1 , whereas if $n = N$, $f_k^{(N,1)} = 1$, due to the normalization of the c_{jk} geometrical factors. The mixing angles are

$$S_k^{(n,m)} = \frac{1}{2} f_k^{(n,m)} \int_{-\infty}^{\infty} \Omega_k(t) dt = \frac{1}{2} f_k^{(n,m)} A_k, \quad (3)$$

where A_k are the pulse areas.

III. RESULTS AND ANALYSIS

Using the Nelder and Mead simplex optimization scheme with linear constraints [65, 66], we optimize the

pulse areas A_k ($k \in [1, N_p]$), and the geometrical parameters e_{jk} ($j \in [1, N], k \in [1, N_p]$), to maximize the fidelity of the gate. In this work $\Omega_k(t)$ are real, so the relative phase between the pulses is fixed as either 0 or π . The algorithm is applied to $\mathcal{N}_T = 10^5$ different initial configurations of the parameters obtained through a uniform distribution within some chosen range. The geometrical factors are constrained such that a minimum value of $|e_{jk}| \geq \sigma$ is imposed. Protocols with smaller σ accept solutions where the influence of the pulse on both qubits at the same time can be smaller, which are related to more separated qubits (or pulse beams with a wider beam waist). We also perform optimizations forcing the positivity of the geometrical factors, $e_{jk} \geq \sigma$ (p-restricted protocols), which we denote by σ^+ .

Fig.(2) shows the pulses and population dynamics starting from the different computational basis for one optimal protocol in a 2-qubit system using three pulses, with $\sigma = 0.1$, which gives an infidelity ($\epsilon = 1 - F$) of $7 \cdot 10^{-7}$ for the \mathcal{P}_{ab} gate. In this particular protocol, with an overall pulse area $A_T = A_1 + A_2 + A_3 = 5.8\pi$, the third pulse is basically used to correct the fidelity of a

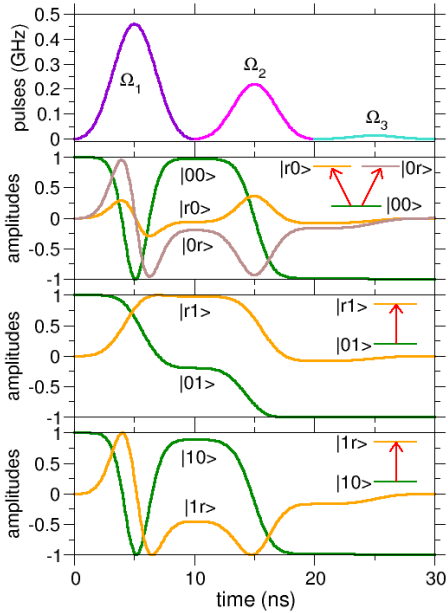


FIG. 2. A particular 3-pulse optimal protocol for the \mathcal{P}_{ab} gate with $\sigma = 0.3$. We show the pulses and amplitudes for the dynamics starting in the different computational basis. The amplitudes in the starting states are real while in the ancillary states are always purely imaginary.

2-pulse sequence. The first pulse acts mainly on the second qubit ($e_{a1}^2 = 0.09$), while the second and third act on the first qubit ($e_{b2}^2 = 0.25$, $e_{b3}^2 = 0.17$). The square of the geometrical factor in the least used qubit measures the degree to which the pulse acts on more than one qubit and hence is an indication of how much the protocol relies on interdependent qubits. The scalar products $\langle e_1|e_2 \rangle = -0.67$, $\langle e_2|e_3 \rangle = 0.57$, $\langle e_1|e_3 \rangle = -0.97$ indicate the correlation among the structural vectors. For this strategy, $\Omega_1(\vec{r}, t)$ and $\Omega_3(\vec{r}, t)$, almost revert their role from the spatial point of view. The first pulse induces a 4π transition from $|00\rangle$, a π transition from $|01\rangle$ and a 2π transition from $|10\rangle$. Only the $|01\rangle$ state goes to the ancillary state $|r1\rangle$ at the end of the first pulse. The second pulse is responsible for a 2π transition from $|00\rangle$ and $|01\rangle$ and a π transition from $|r1\rangle$.

But rather than studying individual results, we want to focus on general trends, for which we analyze common features of the set of all optimal protocols. One of the most interesting conclusions can be obtained by studying the rate of success of the algorithm, which refers to the percentage of initial conditions ($\mathcal{N}_\epsilon/\mathcal{N}_T$) that lead to optimal gates with infidelity smaller than a certain threshold ϵ . The specific curves may change slightly depending on the set of initial conditions, so it is better to compare the curves using a single, very large set.

Fig.3 shows the rate of success for gates \mathcal{P}_{ab} and \mathcal{P}_{abc} for different pulse sequences in 3-qubit systems, where we

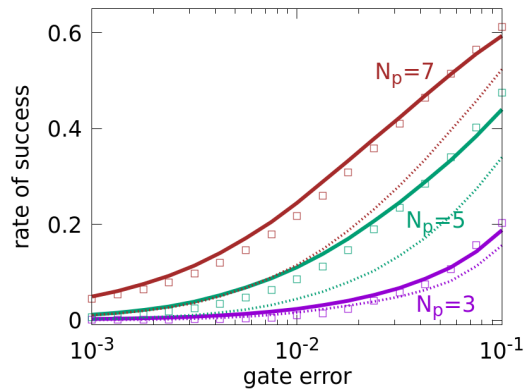


FIG. 3. Rate of success of the optimization as a function of the gate, \mathcal{P}_{ab} (solid lines) and \mathcal{P}_{abc} (squares), for different pulse sequences, imposing $\sigma = 0.1$. In dots we show the result for the \mathcal{P}_{ab} gate imposing $\sigma^+ = 0.1$.

impose $\sigma = 0.1$. Larger pulse sequences use more variational parameters and as expected, have higher rates of success, but one can always find protocols with fidelity greater than 0.99 using only 2-pulse sequences (or 3-pulse sequences in 4-qubit systems). When the number of parameters becomes too large ($N_p \gtrsim 8 + N$) the algorithms do not give significantly better results. The overall behavior is similar for both gates, but in general, there are more successful protocols with low fidelity for the \mathcal{P}_{abc} , particularly when the number of pulses increases, while the opposite is true at the high-fidelity limit. Enforcing positive geometrical factors leads to a decay in the rate of success especially in longer pulse sequences, but this decay is much steeper in the \mathcal{P}_{abc} gate in 3-pulse sequences. This poses interesting questions concerning the main mechanisms used by the different protocols for the different gates.

To classify and visualize the mechanisms of the protocols, we use our recently proposed procedure based on quantum pathways [46]. For each starting subsystem $V^{(n,m)}$, we can write the matrix element of the time evolution operator, $U_{T,11}$ as a contribution of 0-loops (the state of the system after each pulse is the initial state), 1-loops (the population flops to the Rydberg state after one pulse and returns after the next one), d -loops (the population stays in the Rydberg state during the action of one or more consecutive pulses, acting like the 0-loop for the Rydberg states) and 2-loops (the population cycles two times through the excited state). As a reference, the protocol dynamics shown in Fig.2 is a 0-loop for the $V^{(2,1)}$ and $V^{(1,2)}$ subsystems, and a 1-loop for the $V^{(1,1)}$ subsystem. For pulse sequences with $N_p \leq 5$, we do not need to consider extra loops, so $U_{T,11}^{(n,m)} = u_0^{(n,m)} + u_1^{(n,m)} + u_d^{(n,m)} + u_2^{(n,m)}$, where the expressions for the particular matrix elements of the time evolution operators, obtained in [46], are valid for N -qubit systems. Finally, to represent the results in the most simple way, we first define the coordinates of a point

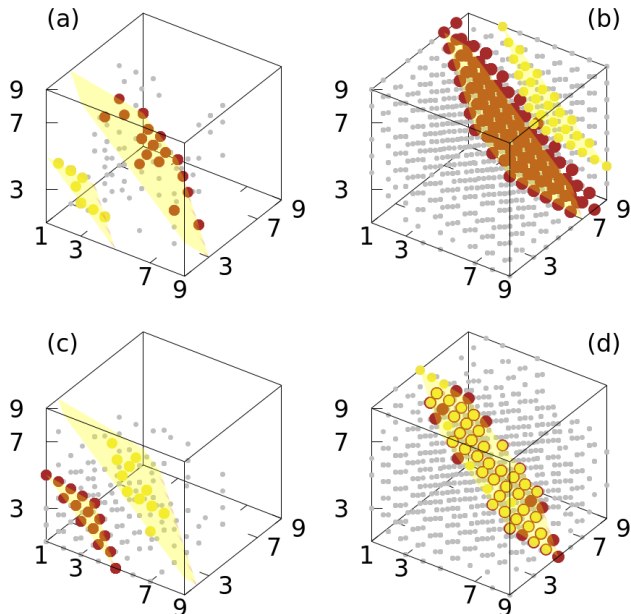


FIG. 4. Diagram showing the most frequent mechanisms for the two-level subsystems $V^{(1,1)}, V^{(1,2)}, V^{(1,3)}$ (top row) and the V subsystems $V^{(2,1)}, V^{(2,2)}, V^{(2,3)}$ for the \mathcal{P}_{ab} gate (brown circles) and the \mathcal{P}_{abc} gate (yellow circles). All used mechanisms for the \mathcal{P}_{ab} gate are shown with gray circles. The first column shows results for 3-pulse sequences; the second, for 5-pulse sequences. The circles have been made of slightly different sizes so that common mechanisms for both gates are mixed brown-yellow circles.

in a square for each subsystem $V^{(n,m)}$,

$$\begin{aligned} x^{(n,m)} &= u_0^{(n,m)} + u_1^{(n,m)} - u_d^{(n,m)} - u_2^{(n,m)} \\ y^{(n,m)} &= u_0^{(n,m)} + u_d^{(n,m)} - u_1^{(n,m)} - u_2^{(n,m)} \end{aligned} \quad (4)$$

and then partition each square into 9 boxes, ranking the mechanism as a number $\omega^{(n,m)} \in [1, 9]$ depending on the box where $(x^{(n,m)}, y^{(n,m)})$ is located [67]. Pure or dominant 0-loops correspond to $\omega = 1$, 1-loops to $\omega = 3$, d-loops to $\omega = 7$, and 2-loops to $\omega = 9$. In between, ω ranks collaborative mechanisms among the closest pure mechanisms, or possibly fully collaborative mechanisms, as is the case of $\omega = 5$.

For a 3-qubit system, for which there are 7 subsystems (plus the decoupled $|111\rangle$ state), we obtain 7 coordinates. The signature of the different entangling gates differs only on the two-level systems, so we expect the prevalent mechanisms for the \mathcal{P}_{ab} and \mathcal{P}_{abc} gates to differ mainly in the dynamics of the two-level subsystems. In Fig.4 we represent the mechanism of each protocol with a point in a cube corresponding to $(\omega^{(1,1)}, \omega^{(1,2)}, \omega^{(1,3)})$ for pulse sequences with 3 (a) and 5 pulses (b), where we have selected protocols with fidelity higher than 0.99 with $\sigma = 0.1$. Although protocols with larger pulse sequences explore all possible mechanisms (shown as gray points in Fig.4 for the \mathcal{P}_{ab} gate) the most prevalent mech-

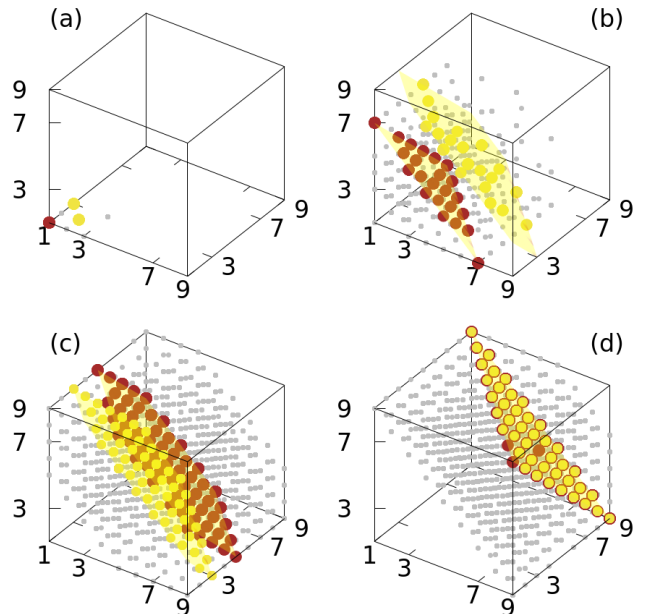


FIG. 5. Diagram showing the most frequent mechanisms for the for the \mathcal{P}_{ab} gate (brown circles) and the \mathcal{P}_{abc} gate (yellow circles) and all observed mechanisms (gray) used by the optimal protocols using (a) 2-pulses, (b) 3-pulses, (c) 4-pulses and (d) 5-pulse sequences. The circles have been made of slightly different sizes so that common mechanisms for both gates are mixed brown-yellow circles.

anisms are clearly different for the two gates (shown as brown points for \mathcal{P}_{ab} and yellow points for \mathcal{P}_{abc}) as they never overlap. These sets vary little for different constraints ($\sigma = 0.3$, p-constrained mechanisms) or different error thresholds ($\epsilon > 10^{-3}$), but depend strongly on the number of pulses.

For 3-pulse sequences, the most used mechanisms lie on a single plane for \mathcal{P}_{abc} , with $\omega^{(1,1)} + \omega^{(1,2)} + \omega^{(1,3)} = 7$. In the \mathcal{P}_{abc} gate, all two-level subsystems play the same role, and this symmetry is passed on to the $\omega^{(1,n)}$ which can be interchanged. The total value $\omega_T^{(1)} = 7$ shows preference for 0-loops and 1-loops or their superposition (but not all the mechanisms within the plane are used equally). This is not the case for the \mathcal{P}_{ab} gate. In the latter, not all dominant mechanism lie on a single plane. In addition, $\omega_T^{(1)}$ is much larger for the \mathcal{P}_{ab} gate, showing preference of d-loops. However, for 5-pulse sequences the prevalent mechanisms for the \mathcal{P}_{abc} gate lie on two planes, while those of the \mathcal{P}_{ab} lie on a single plane. Still, larger $\omega_T^{(1)}$ are used in the \mathcal{P}_{ab} than in the \mathcal{P}_{abc} gate.

The different mechanisms needed to achieve high fidelity protocols used in the $V^{(1,n)}$ subsystems influence the dominant mechanisms explored by the other subsystems as well. In Fig.4(c) and (d) we show the m-cube formed by the set of mechanisms of the V subsystems, $(\omega^{(2,1)}, \omega^{(2,2)}, \omega^{(2,3)})$ for 3 and 5 pulse protocols. While the difference between \mathcal{P}_{ab} and \mathcal{P}_{abc} protocols is obvious

for 3-pulse sequences to the point of no-overlap in the distributions, the differences tend to disappear for longer pulses sequences. Again, most mechanisms lie on one or two planes. The distribution is also different for the preferred mechanisms in $V^{(3,1)}$ for 3-pulse sequences, where $\omega^{(3,1)} = 1$ in \mathcal{P}_{ab} , while $\omega^{(3,1)} = 7$ in \mathcal{P}_{abc} . However, the most used mechanisms tend to coincide again for 5-pulse sequences ($\omega^{(3,1)} = 7$). In general, as the number of pulses increases, the set of mechanisms increases and differences between the gates are less pronounced.

The mechanism analysis for the whole system is difficult to visualize in a single plot for 3-qubit systems, as we need 7 coordinates to characterize every mechanism. We again observe correlations between the set of values for the different kinds of subsystems. To simplify the analysis, in Fig.5 we form a cube with $\omega^{(3,1)}$ in the xy plane, the projection of all $\omega^{(2,j)}$ in the yz plane, and the projection of all $\omega^{(1,j)}$ in the xz plane. The dominant mechanisms in \mathcal{P}_{ab} (brown circles) and \mathcal{P}_{abc} (yellow circles) are shown along the set of other less used mechanisms (gray circles, for a frequency of 30% the most dominant one) for different pulse sequences and $\sigma = 0.1$.

Again, most dominant solutions in both gates line in some particular planes, showcasing the surprising symmetry where the preferred optimal protocols use the same mechanisms regardless of the initial state of the computational basis. That is, if one can find a high fidelity protocol where the dynamics follows a 0-loop from $|000\rangle$ and $|001\rangle$ (or any other subsystem with one excited qubit) and a d -loop starting from $|011\rangle$ (or any other subsystem with two excited qubits), then it is likely that another high fidelity protocol can be found when the dynamics follows a d -loop starting from $|000\rangle$ or $|010\rangle$, while all the other subsystems follow a 0-loop.

Characteristically, we observe that $\omega_T = \omega^{(3,1)} + \omega^{(2,j)} + \omega^{(1,j)}$, with $j = 1, 2, 3$ increases with the number of pulses in the sequence, which correspond to favoring 2-loops over d-loops, and d-loops over 1-loops in the collaborative mechanisms, as one moves from 3 to 5-pulse sequences. The same behavior was observed studying the mechanism of two-qubit systems [46]. We also observe that the set of preferred mechanisms is very different for the \mathcal{P}_{ab} and \mathcal{P}_{abc} gates for short sequences, so they do not share any dominant mechanism for $N_p = 2, 3, 4$. However, the planes approach as the number of pulses increases, and fully overlap for $N_p = 5$.

To evaluate the minimal energy input necessary to operate the gates, we have measured the total pulse area, $A_T = \sum_k A_k$, used in each protocol. We performed optimizations constraining A_T to be smaller than a certain threshold, which was made as small as possible. Fig.6 shows the minimal pulse areas found for the optimal protocols with infidelity smaller than a certain gate error over a large set of initial conditions ($\sim 10^6$), including different pulse sequences and values of σ .

For independent qubits, Jaksch protocol for the CZ gate (\mathcal{P}_{ab}) requires a minimal area of $A_T = 4\pi$ for perfect fidelity [22]. The gray line in Fig.6 gives the theoret-

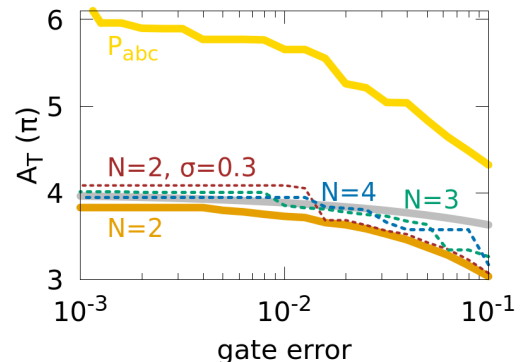


FIG. 6. Minimal pulse area used in the optimal protocols for different gate errors for the \mathcal{P}_{ab} gate implemented in 2, 3, and 4 qubit systems, and for the \mathcal{P}_{abc} gate implemented in 3 qubit systems. For comparison, we also show in the gray line the theoretical minimal area required for independent qubits.

ical value for different fidelities. Using non-independent qubits, the minimal energy can be reduced to 3.8π for high fidelities (better than 0.999) or 3π for low fidelities (better than 0.9). This implies an energy reduction from 3.6% to more than 16% with respect to independent qubits. Strengthening the constraints (e.g. for closer qubits, $\sigma = 0.3$, or demanding positive geometrical factors) implies an increase in the minimal area for high fidelity protocols of no more than 7%. The extra energy is also needed in 3 or 4 qubit systems, but this cost goes to zero for lower fidelity gates.

On the other hand, the dominant mechanisms for the \mathcal{P}_{abc} gate are completely different as the gate requires a minimal energy of roughly 6π for high fidelity protocols (around 2π per qubit, as the sign flip demands Rabi cycling). However, for non-independent qubits at low fidelities, the minimal energy can be substantially reduced. We have obtained protocols with at least 0.9 fidelity with $A_T = 4.3\pi$. While the minimal total areas do not depend on the number of pulses in the \mathcal{P}_{ab} gate, in the case of \mathcal{P}_{abc} , shorter sequences ($N_p \lesssim 4$) perform with an energy penalty.

The constraints on the proximity of the qubits, codified in σ , may have relevant implications on the geometry of the arrays of atoms. To estimate the effect of these constraints, we perform an asymmetric optimization, where we define different values of σ_j (distinguished by the subindex), where σ_1 is the restriction on the minimum allowed geometrical factor of every pulse on every qubit, $|e_{jk}| \geq \sigma_1$, σ_2 is the second allowed minimum value, and σ_j refers to the j th minima. If all minima are the same, each qubit is treated identically, so on average, we expect the distribution of the geometrical factors of the optimal protocols to be similar for all qubits, a feature characteristic of equally separated qubits (e.g. an equilateral triangle or a tetrahedron for 3 and 4 qubit systems). On the other hand, if we chose σ_1 to be much smaller than other $\sigma_{j>1}$, we allow for the distance between two pairs

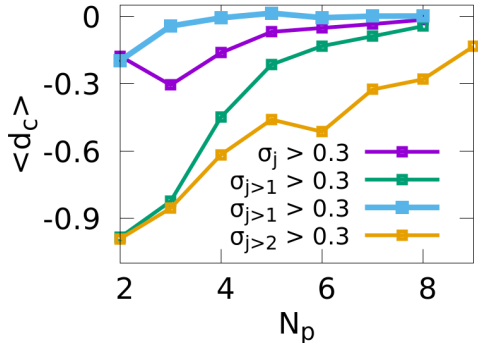


FIG. 7. Average contribution of qubit c in optimal protocols for systems with more than 2-qubits as a function of the number of pulses in the sequence. We show the relative deviation from the uniform contribution, $N e_c^2 - 1$. The blue line is for the \mathcal{P}_{abc} gate, all the others for the \mathcal{P}_{ab} . The orange line gives the average contribution of qubits c and d for a 4-qubit system.

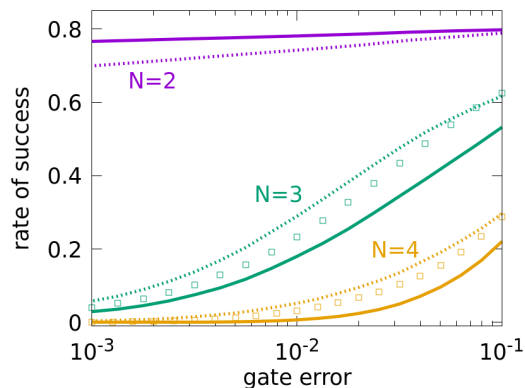


FIG. 8. Rate of success of the optimization for the \mathcal{P}_{ab} gate using 6-pulse sequences in systems with different numbers of qubits. In solid lines, we show the result when $\sigma = 0.1$. We use squares for results with $\sigma_{ab} = 0.3$ where the constraints are imposed on qubits a and b and the field can take any value on the remaining qubits. Dashed lines show the results when $\sigma_1 = 0$ and $\sigma_2 = 0.3$, so the constraints are imposed in two of the three (not initially determined) qubits.

of qubits to be larger, as in asymmetric atomic arrangements (or isosceles triangles and linear arrays in 3-qubit systems).

While the asymmetric optimization allows for some qubits to be used weakly (or not at all) in optimal protocols, the qubits with the smallest σ_j are not predetermined, and moreover, different pulses can use different qubits. On the other hand, we can impose values of σ for specific qubits, leaving other geometrical factors unconstrained, so that those geometrical factors can take any value (including zero). We use σ_{ab} to refer to constraints imposed only on qubits a and b .

Fig.8 shows the rate of success of the optimization of the \mathcal{P}_{ab} gate as a function of the gate error, using 6-pulse sequences in systems with different number of qubits. One always observes a small decay in the rate as σ increases or when more restrictive constraints are imposed, and a large decay when the number of qubits increases. However, asymmetric constraints allow for better results even if σ is larger in a subset of qubits. This can be inferred from Fig.8 by comparing the solid lines ($\sigma = 0.1$) with the dashed lines ($\sigma_{j>1} = 0.3$ for 3-qubit systems, and $\sigma_{j>2} = 0.3$ for 4-qubit systems), where the geometrical factors on one or two qubits are left unconstrained, so they can be zero. One can easily find high-fidelity protocols enforcing the proximity of two of the qubits if at least the pulse does not act (or acts weakly) on the third (and fourth) qubits. Imposing constraints only on qubits a and b (as $\sigma_{ab} = 0.3$) gives the same number of optimal protocols than the more flexible $\sigma_{j>1}$ asymmetric optimization at low fidelities, but less as the fidelity increases.

In 3-qubit systems, we would then expect to obtain a large number of high-fidelity protocols working with linear arrangements of atoms, or using geometries in isosceles triangles over equilateral ones. The asymmetric optimization gives even better improvements when optimizing the \mathcal{P}_{abc} gate. In 3-qubit systems, all the qubits have identical roles for this gate, but more successful optimal protocols are found when each pulse acts only (or mainly) on two qubits at the same time. In 4-qubit systems we apparently do not gain much by reducing the constraints on the parameters of the pulses over two qubits, as the results with $\sigma_{j>2} \geq 0.3$ are not better than those with $\sigma_{j>1} \geq 0.1$ except for very short sequences ($N_p \leq 3$). On the other hand, forcing all pulses to act equally on all qubits results in a steep decay in the performance of the protocols. One would thus expect distorted tetrahedra or square-planar geometries or linear geometries to favor high fidelity protocols over tetrahedron geometries.

To measure how the energy resources are used on average on the different qubits, we define, for each protocol, the relative use of qubit c as

$$d_c = N \left(\frac{1}{N_p} \sum_k e_{3k}^2 \right) - 1. \quad (5)$$

Because \mathbf{e}_k are normalized, if the average of the square of the geometrical factors is $1/N$, the pulses in the optimal protocols act on qubit c as expected from a uniform contribution, and then $d_c = 0$. On the other hand, if $d_c \approx -1$, we can regard qubit c as independent from the other qubits. Finally, we average d_c over all the optimal protocols with fidelity higher than 0.99 and the results are represented as $\langle d_c \rangle$ in Fig.7.

As expected, we observe $\langle d_a \rangle \approx \langle d_b \rangle \approx 0$ in all optimal protocols. In the \mathcal{P}_{ab} gate, qubit c (as well as qubit d in 4-qubit systems) are minimally used for short sequences, implying that $e_{c_k}^2$ barely exceeds the imposed minimal value of the constraint, σ_1^2 (or $\sigma_1^2 + \sigma_2^2$ in 4-qubit sys-

tems). However, all qubits tend to be used equally for large sequences or when $\sigma_j \geq 0.3$. While the constraints could allow for a deviation $\langle d_c \rangle \sim -0.9$, this barely exceeds -0.3 . Optimal protocols for the \mathcal{P}_{abc} gate use all qubits almost equally, except in 2-pulse sequences.

IV. SUMMARY AND CONCLUSIONS

We have developed models for sequences of non-overlapping pulses with control over the spatial degrees of freedom, applied to trapped neutral atoms in ideal conditions. We have explored in great detail the space of optimal protocols that implement CZ-type entangling gates in systems of two or more non-independent qubits, with high fidelity. These qubits can potentially be much closer than in typical traps, forming a denser quantum media that boosts the dipole blockade, so that the gates could in principle operate in the nanosecond regime.

Studying the rate of success of the algorithm as a function of the gate error for different pulse sequences under different constraints, we have evaluated the impact of the proximity of the atoms and, indirectly, the role of the geometry of the arrays in 3 and 4-qubit systems. To characterize the optimal protocols up to 5-pulse sequences, we have proposed a mechanism analysis based on pathways that connect the initial computational state of the qubit with the final state, in terms of 0-, 1-, d-, and 2-loops. We have approximately ranked the solutions in terms of pure mechanisms, or their combinations, characterizing each protocol by a point in a cube.

Even slight changes in the gate have a strong impact on the preferred mechanisms, to the point that the set of optimal mechanisms mostly used to implement the \mathcal{P}_{ab} and \mathcal{P}_{abc} gates barely overlap in short sequences. The minimal energy requirements and the relative use of the qubits is also very different. In the entangling 2-qubit gate, the pulses have less impact on the additional qubits in the set-up, while they act equally on all qubits for the 3-qubit gate. However, these differences drop when the number of pulses in the sequence, and hence the number of optimization parameters, increases. Measuring the energy by the accumulated pulse area of all the sequence, the first gate requires a minimum of 4π to operate with independent qubits, while the latter needs at least 6π . However, when the pulses act on two or more qubits at the same time, the minimal total area can be substantially reduced in gates that operate at low fidelities. This

is especially so in the case of \mathcal{P}_{abc} , when the area is distributed over 5 or more pulses.

Asymmetric optimizations show that it is easier to find optimal protocols with different characteristic distances (different σ_j). Hence, slightly asymmetric atomic arrangements in isosceles triangles (or linear configurations) and distorted tetrahedra (or squares) allow many more high-fidelity protocols than the more symmetric structures.

We have shown that it is always possible to find high-fidelity protocols even with short sequences in systems with more than 2-qubits. The rate of success is smaller when the number of pulses diminishes or the qubits are closer, with worse results when we impose large fields everywhere. Given that the number of parameters that control the system raises with the number of qubits and pulses as $N \times N_p$, while the gate implementation requires an exponential increase of constraints, 2^N , it is somehow surprising that one can obtain relatively high fidelity solutions ($\epsilon < 0.99$) using $N_p \sim N + 1$. We have also found that by increasing the allowed pulse areas one can find solutions even for highly interacting qubits.

The general findings in this work allow us to speculate that one could work with denser arrays of qubits boosting the dipole blockade, accelerating the operating time of the gates by almost two orders of magnitude, and hence nearly reaching the nanosecond time-scales. Fast gates are inherently more robust to decoherent effects. Preliminary studies show that the gates are also relatively robust to the thermal motion of the atoms and fluctuations in the pulse intensities. However, further studies are needed to assess the effect of nonlinear effects in the Hamiltonian, not included in our models, as well as the practical limitations in moving the atoms or using complex light structures in the spatial-domain, instead of the time-domain.

ACKNOWLEDGEMENTS

This research was supported by the Quantum Computing Technology Development Program (NRF-2020M3E4A1079793). IRS thanks the BK21 program (Global Visiting Fellow) for the stay during which this project started and the support from MINECO PID2021-122796NB-I00. SS acknowledges support from the Center for Electron Transfer funded by the Korea government(MSIT)(NRF-2021R1A5A1030054)

-
- [1] F. Nogrette, H. Labuhn, S. Ravets, D. Barredo, L. Béguin, A. Vernier, T. Lahaye, and A. Browaeys, Single-atom trapping in holographic 2d arrays of microtraps with arbitrary geometries, *Phys. Rev. X* **4**, 021034 (2014).
- [2] D. Barredo, S. de Léséleuc, V. Lienhard, T. Lahaye, and A. Browaeys, An atom-by-atom as-

- sembler of defect-free arbitrary two-dimensional atomic arrays, *Science* **354**, 1021 (2016), <https://www.science.org/doi/pdf/10.1126/science.aah3778>.
- [3] J. Wilson, S. Saskin, Y. Meng, S. Ma, R. Dilip, A. Burgers, and J. Thompson, Trapping alkaline earth rydberg atoms optical tweezer arrays, *Physical Review Letters* **128**, 10.1103/PhysRevLett.128.033201 (2022).

- [4] A. P. Burgers, S. Ma, S. Saskin, J. Wilson, M. A. Alarcón, C. H. Greene, and J. D. Thompson, Controlling rydberg excitations using ion-core transitions in alkaline-earth atom-tweezer arrays, *PRX Quantum* **3**, 020326 (2022).
- [5] W. Lee, H. Kim, and J. Ahn, Three-dimensional rearrangement of single atoms using actively controlled optical microtraps, *Opt. Express* **24**, 9816 (2016).
- [6] D. Comparat and P. Pillet, Dipole blockade in a cold rydberg atomic sample, *J. Opt. Soc. Am. B* **27**, A208 (2010).
- [7] D. Tong, S. M. Farooqi, J. Stanojevic, S. Krishnan, Y. P. Zhang, R. Côté, E. E. Eyler, and P. L. Gould, Local blockade of rydberg excitation in an ultracold gas, *Phys. Rev. Lett.* **93**, 063001 (2004).
- [8] E. Urban, T. A. Johnson, T. Henage, L. Isenhower, D. D. Yavuz, T. G. Walker, and M. Saffman, Observation of rydberg blockade between two atoms, *Nature Physics* **5**, 110 (2009).
- [9] A. Gaëtan, Y. Miroshnychenko, T. Wilk, A. Chotia, M. Viteau, D. Comparat, P. Pillet, A. Browaeys, and P. Grangier, Observation of collective excitation of two individual atoms in the rydberg blockade regime, *Nature Physics* **5**, 115 (2009).
- [10] J. D. Pritchard, D. Maxwell, A. Gauguier, K. J. Weatherill, M. P. A. Jones, and C. S. Adams, Cooperative atom-light interaction in a blockaded rydberg ensemble, *Phys. Rev. Lett.* **105**, 193603 (2010).
- [11] H. Levine, A. Keesling, A. Omran, H. Bernien, S. Schwartz, A. S. Zibrov, M. Endres, M. Greiner, V. Vuletić, and M. D. Lukin, High-fidelity control and entanglement of rydberg-atom qubits, *Phys. Rev. Lett.* **121**, 123603 (2018).
- [12] Y. Zeng, P. Xu, X. He, Y. Liu, M. Liu, J. Wang, D. J. Papoular, G. V. Shlyapnikov, and M. Zhan, Entangling two individual atoms of different isotopes via rydberg blockade, *Phys. Rev. Lett.* **119**, 160502 (2017).
- [13] H. Jo, Y. Song, M. Kim, and J. Ahn, Rydberg atom entanglements in the weak coupling regime, *Phys. Rev. Lett.* **124**, 033603 (2020).
- [14] T. Wilk, A. Gaëtan, C. Evellin, J. Wolters, Y. Miroshnychenko, P. Grangier, and A. Browaeys, Entanglement of two individual neutral atoms using rydberg blockade, *Phys. Rev. Lett.* **104**, 010502 (2010).
- [15] T. M. Graham, Y. Song, J. Scott, C. Poole, L. Phuttitarn, K. Jooya, P. Eichler, X. Jiang, A. Marra, B. Grinkemeyer, M. Kwon, M. Ebert, J. Cherek, M. T. Lichtman, M. Gillette, J. Gilbert, D. Bowman, T. Ballance, C. Campbell, E. D. Dahl, O. Crawford, N. S. Blunt, B. Rogers, T. Noel, and M. Saffman, Multi-qubit entanglement and algorithms on a neutral-atom quantum computer, *Nature* **604**, 457 (2022).
- [16] K. M. Maller, M. T. Lichtman, T. Xia, Y. Sun, M. J. Piotrowicz, A. W. Carr, L. Isenhower, and M. Saffman, Rydberg-blockade controlled-not gate and entanglement in a two-dimensional array of neutral-atom qubits, *Phys. Rev. A* **92**, 022336 (2015).
- [17] X. L. Zhang, L. Isenhower, A. T. Gill, T. G. Walker, and M. Saffman, Deterministic entanglement of two neutral atoms via rydberg blockade, *Phys. Rev. A* **82**, 030306 (2010).
- [18] C. J. Picken, R. Legaie, K. McDonnell, and J. D. Pritchard, Entanglement of neutral-atom qubits with long ground-rydberg coherence times, *Quantum Science and Technology* **4**, 015011 (2018).
- [19] V. S. Malinovsky and I. R. Sola, Quantum control of entanglement by phase manipulation of time-delayed pulse sequences. i, *Phys. Rev. A* **70**, 042304 (2004).
- [20] V. S. Malinovsky and I. R. Sola, Quantum phase control of entanglement, *Phys. Rev. Lett.* **93**, 190502 (2004).
- [21] V. S. Malinovsky and I. R. Sola, Phase-controlled collapse and revival of entanglement of two interacting qubits, *Phys. Rev. Lett.* **96**, 050502 (2006).
- [22] D. Jaksch, J. I. Cirac, P. Zoller, S. L. Rolston, R. Côté, and M. D. Lukin, Fast quantum gates for neutral atoms, *Phys. Rev. Lett.* **85**, 2208 (2000).
- [23] L. Isenhower, M. Saffman, and K. Mølmer, Multibit cknnot quantum gates via rydberg blockade, *Quantum Information Processing* **10**, 755 (2011).
- [24] M. D. Lukin, M. Fleischhauer, R. Cote, L. M. Duan, D. Jaksch, J. I. Cirac, and P. Zoller, Dipole blockade and quantum information processing in mesoscopic atomic ensembles, *Phys. Rev. Lett.* **87**, 037901 (2001).
- [25] H. Levine, A. Keesling, G. Semeghini, A. Omran, T. T. Wang, S. Ebadi, H. Bernien, M. Greiner, V. Vuletić, H. Pichler, and M. D. Lukin, Parallel implementation of high-fidelity multiqubit gates with neutral atoms, *Phys. Rev. Lett.* **123**, 170503 (2019).
- [26] S. R. Cohen and J. D. Thompson, Quantum computing with circular rydberg atoms, *PRX Quantum* **2**, 030322 (2021).
- [27] X.-F. Shi, Quantum logic and entanglement by neutral rydberg atoms: methods and fidelity, *Quantum Science and Technology* **7**, 023002 (2022).
- [28] X.-F. Shi, Deutsch, toffoli, and cnot gates via rydberg blockade of neutral atoms, *Phys. Rev. Applied* **9**, 051001 (2018).
- [29] D. Paredes-Barato and C. S. Adams, All-optical quantum information processing using rydberg gates, *Phys. Rev. Lett.* **112**, 040501 (2014).
- [30] C. S. Adams, J. D. Pritchard, and J. P. Shaffer, Rydberg atom quantum technologies, *Journal of Physics B: Atomic, Molecular and Optical Physics* **53**, 012002 (2019).
- [31] V. S. Malinovsky, I. R. Sola, and J. Vala, Phase-controlled two-qubit quantum gates, *Phys. Rev. A* **89**, 032301 (2014).
- [32] M. H. Goerz, T. Calarco, and C. P. Koch, The quantum speed limit of optimal controlled phasegates for trapped neutral atoms, *Journal of Physics B: Atomic, Molecular and Optical Physics* **44**, 154011 (2011).
- [33] M. Morgado and S. Whitlock, Quantum simulation and computing with rydberg-interacting qubits, *AVS Quantum Science* **3**, 10.1116/5.0036562 (2021).
- [34] J. T. Young, P. Bienias, R. Belyansky, A. M. Kaufman, and A. V. Gorshkov, Asymmetric blockade and multiqubit gates via dipole-dipole interactions, *Phys. Rev. Lett.* **127**, 120501 (2021).
- [35] M. Saffman, I. I. Beterov, A. Dalal, E. J. Pérez, and B. C. Sanders, Symmetric rydberg controlled- z gates with adiabatic pulses, *Phys. Rev. A* **101**, 062309 (2020).
- [36] M. A. Nielsen and I. L. Chuang, *Quantum Computation and Quantum Information: 10th Anniversary Edition* (Cambridge University Press, 2010).
- [37] M. Saffman, T. G. Walker, and K. Mølmer, Quantum information with rydberg atoms, *Rev. Mod. Phys.* **82**, 2313 (2010).
- [38] A. Browaeys and T. Lahaye, Many-body physics with individually controlled rydberg atoms, *Nature Physics* **16**,

- 132 (2020).
- [39] I. Averbukh and M. Shapiro, Optimal squeezing of molecular wave packets, *Phys. Rev. A* **47**, 5086 (1993).
- [40] T. Szakács, B. Amstrup, P. Gross, R. Kosloff, H. Rabitz, and A. Lörincz, Locking a molecular bond: A case study of csi, *Phys. Rev. A* **50**, 2540 (1994).
- [41] R. S. Judson and H. Rabitz, Teaching lasers to control molecules, *Phys. Rev. Lett.* **68**, 1500 (1992).
- [42] C. Brif, R. Chakrabarti, and H. Rabitz, Control of quantum phenomena: past, present and future, *New Journal of Physics* **12**, 075008 (2010).
- [43] F. Sauvage and F. Mintert, Optimal control of families of quantum gates, *Phys. Rev. Lett.* **129**, 050507 (2022).
- [44] M. Khazali, All-optical quantum information processing via a single-step rydberg blockade gate, *Opt. Express* **31**, 13970 (2023).
- [45] I. R. Sola, V. S. Malinovsky, J. Ahn, S. Shin, and B. Y. Chang, Two-qubit atomic gates: spatio-temporal control of rydberg interaction, *Nanoscale* **15**, 4325 (2023).
- [46] I. R. Sola, S. Shin, and B. Y. Chang, Finding, mapping, and classifying optimal protocols for two-qubit entangling gates (2023), arXiv:quant-ph/2304.14322.
- [47] J. P. Palao and R. Kosloff, Optimal control theory for unitary transformations, *Phys. Rev. A* **68**, 062308 (2003).
- [48] M. H. Goerz, D. M. Reich, and C. P. Koch, Optimal control theory for a unitary operation under dissipative evolution, *New Journal of Physics* **16**, 055012 (2014).
- [49] T. Caneva, T. Calarco, and S. Montangero, Chopped random-basis quantum optimization, *Phys. Rev. A* **84**, 022326 (2011).
- [50] S. Scotto, *Rubidium vapors in high magnetic fields*, Ph.D. thesis (2016).
- [51] T. F. Gallagher, *Rydberg Atoms*, Cambridge Monographs on Atomic, Molecular and Chemical Physics (Cambridge University Press, 1994).
- [52] S. Rice and M. Zhao, *Optical Control of Molecular Dynamics* (John Wiley & Sons, Ltd, 2000).
- [53] M. Shapiro and P. Brummer, *Quantum Control of Molecular Processes* (John Wiley & Sons, Ltd, 2011).
- [54] B. W. Shore, *Manipulating Quantum Structures Using Laser Pulses* (Cambridge University Press, 2011).
- [55] C. M. Tesch, L. Kurtz, and R. de Vivie-Riedle, Applying optimal control theory for elements of quantum computation in molecular systems, *Chemical Physics Letters* **343**, 633 (2001).
- [56] C. M. Tesch and R. de Vivie-Riedle, Quantum computation with vibrationally excited molecules, *Phys. Rev. Lett.* **89**, 157901 (2002).
- [57] J. P. Palao, R. Kosloff, and C. P. Koch, Protecting coherence in optimal control theory: State-dependent constraint approach, *Phys. Rev. A* **77**, 063412 (2008).
- [58] S. J. Glaser, U. Boscain, T. Calarco, C. P. Koch, W. Köckenberger, R. Kosloff, I. Kuprov, B. Luy, S. Schirmer, T. Schulte-Herbrüggen, D. Sugny, and F. K. Wilhelm, Training schrödinger’s cat: quantum optimal control, *The European Physical Journal D* **69**, 279 (2015).
- [59] C. P. Koch, U. Boscain, T. Calarco, G. Dirr, S. Filipp, S. J. Glaser, R. Kosloff, S. Montangero, T. Schulte-Herbrüggen, D. Sugny, and F. K. Wilhelm, Quantum optimal control in quantum technologies. strategic report on current status, visions and goals for research in europe, *EPJ Quantum Technology* **9**, 19 (2022).
- [60] M. M. Müller, D. M. Reich, M. Murphy, H. Yuan, J. Vala, K. B. Whaley, T. Calarco, and C. P. Koch, Optimizing entangling quantum gates for physical systems, *Phys. Rev. A* **84**, 042315 (2011).
- [61] L. S. Theis, F. Motzoi, F. K. Wilhelm, and M. Saffman, High-fidelity rydberg-blockade entangling gate using shaped, analytic pulses, *Phys. Rev. A* **94**, 032306 (2016).
- [62] M. V. R. K. Murty, A simple way of demonstrating the phase reversals in the tem10, tem20, tem30 modes of a gas laser source, *Appl. Opt.* **3**, 1192 (1964).
- [63] A. Forbes, M. de Oliveira, and M. R. Dennis, Structured light, *Nature Photonics* **15**, 253 (2021).
- [64] H. Rubinsztein-Dunlop, A. Forbes, M. V. Berry, M. R. Dennis, D. L. Andrews, M. Mansuripur, C. Denz, C. Alpmann, P. Banzer, T. Bauer, E. Karimi, L. Marrucci, M. Padgett, M. Ritsch-Marté, N. M. Litchinitser, N. P. Bigelow, C. Rosales-Guzmán, A. Belmonte, J. P. Torres, T. W. Neely, M. Baker, R. Gordon, A. B. Stilgoe, J. Romero, A. G. White, R. Fickler, A. E. Willner, G. Xie, B. McMorran, and A. M. Weiner, Roadmap on structured light, *Journal of Optics* **19**, 013001 (2016).
- [65] J. A. Nelder and R. Mead, A Simplex Method for Function Minimization, *The Computer Journal* **7**, 308 (1965), <https://academic.oup.com/comjnl/article-pdf/7/4/308/1013182/7-4-308.pdf>.
- [66] M. J. D. Powell, Direct search algorithms for optimization calculations, *Acta Numerica* **7**, 287–336 (1998).
- [67] Defining the floor integers (greatest integer smaller than the real number) $\lfloor x^{(n,m)} \rfloor = \lfloor l(x^{(n,m)} + 1)/2 \rfloor + 1$, $\lfloor y^{(n,m)} \rfloor = \lfloor l(y^{(n,m)} + 1)/2 \rfloor + 1$ (where $l = 3$ is the number of divisions of each m-square side, $\lfloor x^{(n,m)} \rfloor, \lfloor y^{(n,m)} \rfloor \in [1, 3]$), we call $\omega^{(n,m)} = \lfloor y^{(n,m)} \rfloor + l(\lfloor x^{(n,m)} \rfloor - 1)$ the number that ranks the mechanism for each $V^{(n,m)}$.